CHALMERS

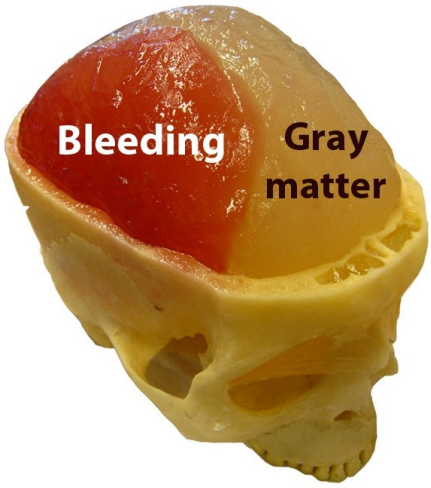

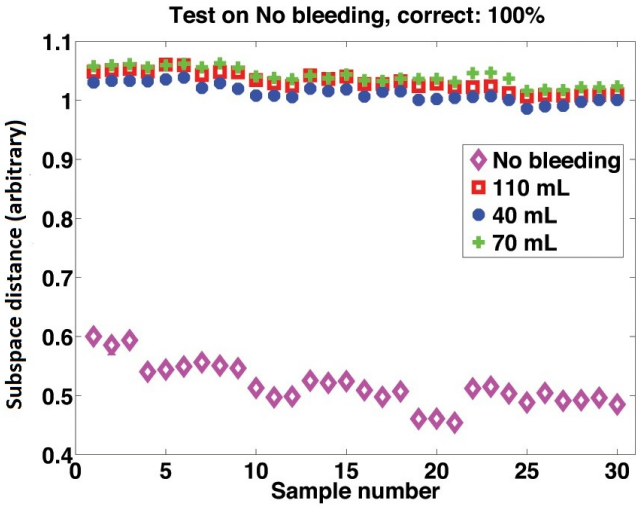

Detecting traumatic intracranial bleedings in a brain phantom using microwave technology

Master's Thesis

Malik Ahzaz Ahmad

Department of Signal & Systems
Chalmers University of Technology
Gothenburg, Sweden 2012
Report No: EX042/2012

Abstract

Traumatic Brain Injury (TBI) is one of the major causes of death due to injury and frequently occurs in road traffic accidents, assaults, sports injuries, etc. It has been estimated that TBI will become a leading cause of death in the near future. Intracranial bleedings is one of the most severe complications of TBI, and need to be detected and treated at an early phase to save the lives of these patients.

The objective of this thesis was to make a realistic human brain phantom and assess the potential of Microwave Technology (MWT) for detecting intracranial bleedings due to head injury. MWT can detect bleedings based on the difference between the dielectric properties of blood and brain tissue. In this thesis we modeled a particularly common and dangerous type of intracranial bleeding, subdural hematoma, following descriptions of typical shape and clinically relevant size in the literature. Measurements were performed using a Microwave Helmet (MWH) developed by researchers at Chalmers University in collaboration with Medfield Diagnostics AB.

Experiments were setup and conducted in the two labs at Chalmers and Medfield Diagnostics. Major series of experiments included measurements on bleeding and without bleeding phantoms in plastic buckets and in a human cranium. Initially different sizes of bleedings were tested in the plastic buckets, followed by creating bleeding phantoms of sizes 40, 70 and 110 mL inside the human cranium. The bleedings in the human cranium were made by cutting away a portion of the brain phantom with a scalpel and refilling with bleeding phantom. The measurements on the cranium were performed using the MWH consisting of 12 antennas, and the measurements on the plastic buckets were done using two antennas attached to the buckets' sides. The measurement order was randomized when possible. Furthermore, potential interfering factors such as movements of the MWH/antennas and the cables, presence of a mobile phone on call close to the experimental setup, and presence of a person close to the setup, were also investigated. A classification algorithm was used to distinguish between phantoms without bleeding and phantoms with bleedings of different sizes.

The classification results both for buckets and human cranium experiments showed that there was a clear difference between without bleeding and bleeding phantoms. The classification results for the human cranium phantom indicate that subdural hematoma of clinically relevant sizes can be detected using MWT. The tests on possibly interfering factors showed that human presence and mobile signals close to the experimental setup had clear effects. However, other factors did not show any clear interference.

The results indicate that MWT has high potential for detecting intracranial hematomas, and may become a future complement to Computed Tomography (CT) for ambulatory use. The advantages like its low cost, small size and non ionizing radiation make this technology very attractive to use in an emergency setting.

Acknowledgements

I am very grateful to my supervisor Stefan Candefjord for providing me opportunity for doing this thesis. I really admire your efforts and support during the whole thesis. You have not only provided my great guidance and support but also gave me lot of confidence by constant encouragement throughout the thesis. I am more specifically very thankful to you for your help in making phantoms, performing experiments, writing report and presentation. Without your help it would be very hard to conduct this thesis.

I am thankful to Stefan Kidborg and Patrick Dahlqvist at Medfield Diagnostics for providing me their time and resources for conducting experiments. The technical support and guidance from Stefan Kidborg was very useful in conducting successful experiments. I am also thankful to Professor Tomas McKelvey and Yinan Yu at Chalmers University for their help with classification algorithm and very useful discussions. I would also like to express my gratitude to my examiner Andreas Fhager and his colleagues Xuezhi Zeng, Hana Trefna and Johanna Gellermann at Chalmers University for their support and guidance. I am also thankful to all staff at MedTech West for providing me a working place and resources for work.

Malik Ahzaz Ahmad
Gothenburg, June 2012

Contents

List of Figures

List of Tables

Abbreviations

CT	Computed Tomography
EDH	Epidural Hematoma
EMS	Emergency Medical Staff
ICH	Intracerebral Hematoma
MRI	Magnetic Resonance Imaging
MWH	Microwave Helmet
MWT	Microwave Technology
SAH	Subarachnoid Hemorrhage
SDH	Subdural Hematoma
TBI	Traumatic Brain Injury
VNA	Vector Network Analyzer

1

Introduction

Traumatic Brain Injury (TBI) is one of the leading causes of death and disability [1]. 10 million people are affected by it annually throughout the world, and 15 % are moderately or severely injured [1]. Road traffic injuries, gun shots, injury during sports, etc. are the major causes for TBI [2]. TBI can occur when the head strikes an object; the resulting forces travel through the skull bone and the brain (Figure 1.1). TBI can also arise when the head is exposed to violent acceleration, such as in motor vehicle crashes [3]. It has been estimated that by year 2020, TBI will become the third leading cause of death and disability in the world [1].

The grade of severity of TBI can be classified clinically using the Glasgow Coma Scale, by assessing the level of consciousness of a patient [4]. Chronologically TBI is divided into primary and secondary injury. Primary injuries results from direct impact, whereas secondary injuries are the further complications or consequences of the primary injury. TBI can also be classified based on location (intra or extra axial) and extent of the injuries (open or closed). Intra-axial injuries are located inside the brain and include intracerebral hematoma, cortical contusion, traumatic axonal injury, and cerebrovascular injury. Extra-axial injuries are epidural, subdural, subarachnoid and intraventricular hemorrhages [1].

Early detection and treatment of severe TBI is important to save lives of these patients, and to minimize the number of severely disabled among the survivors [5]. In particular, intracranial hematoma is the most critical complication of TBI and it causes problems in 25 to 45 % of severe TBI cases, 3 to 12% of moderate TBI and around 1 in 500 patients with mild TBI [5]. Massive intracranial bleedings or bleedings in some specific parts of brain like brain stem can cause death or permanent paralysis. Large hematomas must be evacuated promptly since delay to treatment decreases the chances for the patient to survive [5].

Computed Tomography (CT) is widely used clinically to detect TBI. However, CT devices are relatively large and not suited for ambulatory use. A possible complement

to CT for ambulatory use is microwave technology, which has shown promising results for detecting bleedings in stroke patients [6, 7, 8]. If intracranial hematoma could be detected already in the ambulance many lives may be saved, since minimizing the time to surgery is of crucial importance [5]. This thesis will evaluate the potential for using microwave technology to detect intracranial hematomas.

1.1 Different kinds of Traumatic Brain Injuries

A number of different complications can occur in TBI. This section lists some of the most common, with focus on intracranial hematomas.

1.1.1 Skull fractures

In this type of head injury the pattern of fracture on skull explains how injury occurred. Based on these patterns they are classified in different types. Fractures are found in 25% of head injuries cases at autopsy [2].

1.1.2 Contusions

Contusion is a bruise of a brain surface in which blood vessels are broken and blood is leaked into brain tissues. There are further different types of contusions and those depend upon the state of the victims body position, and movements at the time of application of force causing injury [2].

1.1.3 Epidural hematoma

Epidural Hematoma (EDH) is observed in 1 to 4% of TBI patients and is usually formed when there is a bleeding between the space of dura mater and skull (Figure 1.2, top left). It occurs due to direct impact, which is also the reason that it is easy for doctors to predict the progression of EDH as compared to Subdural Hematoma (SDH) [1].

1.1.4 Subdural hematoma

SDH is formed when bleedings occur in subdural space [1]. It is observed in about 10 to 20% of TBI patients, often due to traffic accidents, offensive aggression and in accidental sport falls. SDH are generally not directly caused by fracture of skull, as often is the case for EDH. It has a higher mortality rate than EDH, and is an important cause of death in severely injured patients [1]. SDH most commonly occur when the cortical veins in the subdural space are broken; the resulting bleeding expands the subdural space between dura and arachnoid (Figure 1.2). SDH is more commonly located at the countercoup location, but it can also be observed at the coup location (Figure 1.1) [1].

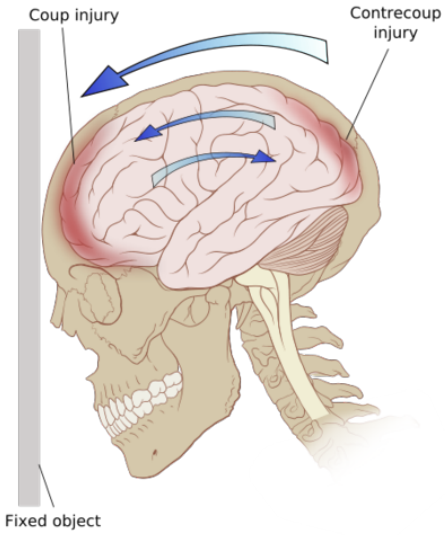

Figure 1.1: Schematic drawing showing the coup and contrecoup TBI locations. (Picture from Wikipedia, http://en.wikipedia.org/wiki/File:Contrecoup.svg, April 2012)

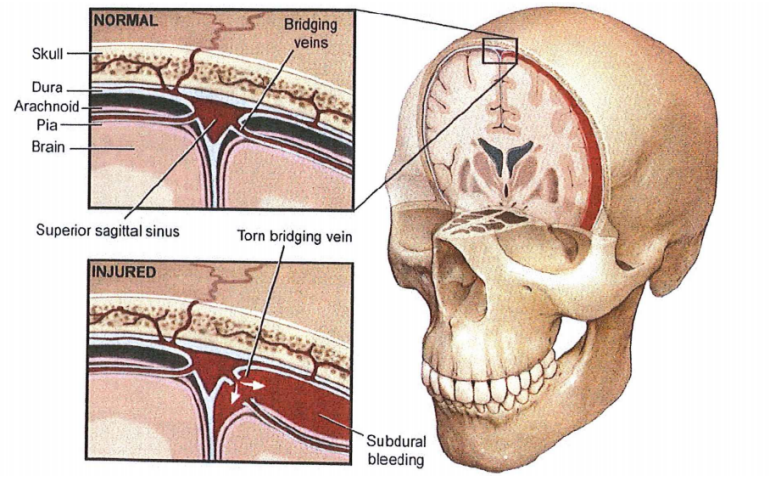

Figure 1.2: Acute SDH. Schematic drawing of the most common mechanism of the SDH. (Reprinted from Head trauma, 20, A.D. Gean, N. J. Fischlbein, Head trauma, 527-556, Copyright (2010), with permission from Elsevier)

1.1.5 Intracerebral hematoma

Intracerebral Hematoma (ICH) normally occurs when a blood vessel in the brain breaks and causes bleeding in different parts of brain like basal ganglia, cerebellum and brain stem. ICH is observed in about 20% of patients with acute SDH, but it is not usually accompanied by EDH [2]. ICH is produced in 0.4–9% of patients having intracranial hematomas, and can be present in about 40% of patients in autopsy [2]. ICH has a relatively high mortality rate. Different studies have showed total mortality rates of 30–40% after 1 month, around 50% after 1 year and 75% after 11 years [9].

1.1.6 Subarachnoid hemorrhage

Subarachnoid Hemorrhage (SAH) is caused when there is bleeding in the subarachnoid space due to TBI or cerebral aneurysm, i.e. weak blood vessels in the brain swell like a balloon and eventually burst [10]. SAH is usually present near the fracture of skull or contusion and occurs in up to 11% of TBI [1].

1.2 Treatment of intracranial hematomas

Emergency Medical Staff (EMS) personnel are most of time first to treat the patients with head injury and transport them to hospital. EMS staff treat TBI patients according to predefined guidelines as in [11]. As TBI occurs, the EMS first make an immediate assessment and stabilize the patients airways and circulation [12]. Following that an immediate CT scan is arranged to investigate the extent of secondary injuries. Monitoring of intracranial pressure is also done and if necessary treatment is given to reduce the intracranial pressure [11].

Another technique used by clinicians is to reduce cerebral perfusion pressure. One study showed that 80 % of patients presented good signs of recovery when cerebral perfusion pressure was maintained at 70 mm Hg by various methods [13].

Depending upon the size of the hemorrhage and on which part of brain it has occurred there are different complications. Patients can have headache, loose consciousness, loss of vision, and many other complications. Surgical management of posttraumatic intracranial hematomas are generally based on certain guidelines as in [5]. In USA alone 100,000 patients require surgical procedures for posttraumatic intracranial hematoma [5]. Lessions which are less in volume (<25 cm^3) are not usually evacuated but generally decisions are made to evacuate lessions which are >50 cm^3; however, it is difficult to make decisions for carrying out surgery for lesions of intermediate size [5].

1.3 Techniques for diagnosing Traumatic Brain Injuries

The goal of all techniques for detection and imaging is to predict the progression of TBI. Each technique has advantages for describing specific types of TBI, but CT is always the primary choice when dealing with TBI [1]. The reason for this is its high

detection speed, availability and high sensitivity. There are variants of CT like CT angiography, CT perfusion and Dual CT, each employed for different types of TBI. Magnetic Resonance Imaging (MRI) is used in cases when results are not clear with CT and its recommended use also depend upon the patient's symptoms. MRI is far better than CT in explaining certain types of TBI that cannot be detected by CT at all [1]. However, due to patient claustrophobia, high costs, long measurement times, and its sensitivity to patient movements MRI is used less frequently [1].

There are some upcoming technologies that aim for detecting intracranial bleedings. The Infrascanner is a near infrared spectroscopy (NIRS) device that measures the absorption of light. The transmitter and the receiver are positioned on the same side of the head. The advantages with this device are that it is portable, non-invasive and has very low cost [14]. Furthermore, this device can give good results even for small bleeding volumes down to 3.5 mL. The main limitation with this device is that it cannot detect bleedings that are more than approximately 2.5 cm from the brain surface [15].

1.4 Microwave technology

The basic principle of detection behind the technique used in this study is based on the high difference of dielectric properties such as permittivity between blood and brain tissue [16, 17]. The advantages with MWT in comparison to above mentioned approaches is that it may be more cost effective, safe for the patient, measurement times are short and that the device could be made small and easily portable [18]. Furthermore, MWT has high potential for detecting deep-lying bleedings in brain, in contrast to the Infrascanner NIRS based technique. Since MWT uses several transmitting and receiving antennas placed around the head, bleedings can be detected at larger distances from the brain surface [19].

MWT emits non-ionizing radiation in contrast to CT, which could possibly help to reduce the use of CT for patients which have less severe head injuries. The excessive use of CT has raised the risks of cancer especially in child treatment [20, 21, 22, 23]. Hence due to the important advantages of safety and portability MWT may be used as a complement to CT in the future, by reducing doses of CT and providing extra aid to emergency staff by on site examination.

1.5 Aims

The aim of this thesis was to evaluate the potential of using MWT for detecting typical intracranial bleedings due to acute head injuries. A Microwave Helmet (MWH) for microwave measurements of the head was assembled and used, and a phantom model of a traumatic bleeding was developed using a human cranium. The thesis focused on detection of SDH, which as explained are of special importance in TBI management. Furthermore, to test the accuracy and robustness of the experimental setup, the effect from several interfering factors were also investigated.

2

Materials and methods

In this chapter practical details of the thesis work are included. It explains the experimental setup used, how the phantoms were made, how the experiments were performed, and the data analysis.

2.1 Experimental setup

Experimental work was performed at two different labs, situated at Department of Signal and Systems, Chalmers University of Technology and Medfield Diagnostics. Most measurements were performed at Medfield Diagnostics. Some measurements were performed using only two antennas, whereas the final measurements were performed using the MWH.

2.1.1 Assembling the microwave helmet

The MWH was assembled using new copies of parts constructed by Medfield Diagnostics. Figure 2.1 (b) shows the MWH after it had been assembled. The MWH body was made of plastic material and 12 antennas could be fitted on it. The antennas were developed in-house [24]. All antennas were properly tested before placing them in the MWH. The MWH was used at both labs where experiments were performed.

Each antenna was protected by a shrinkable plastic material and placed inside the MWH at their respective numbered places (Figure 2.1 (a)). The antennas could be attached and detached from the MWH using plastic nails. A water bag was attached on each antenna to provide efficient coupling between the antenna and object measured, by high quality dual stitching tape. The water bags were specially designed so that water could easily flow between them. The MWH could be firmly attached to the measurement object by adjusting the water level in the water bags. Special care was taken to attach the water bags to the MWH in a way so that the water flow between them was not obstructed.

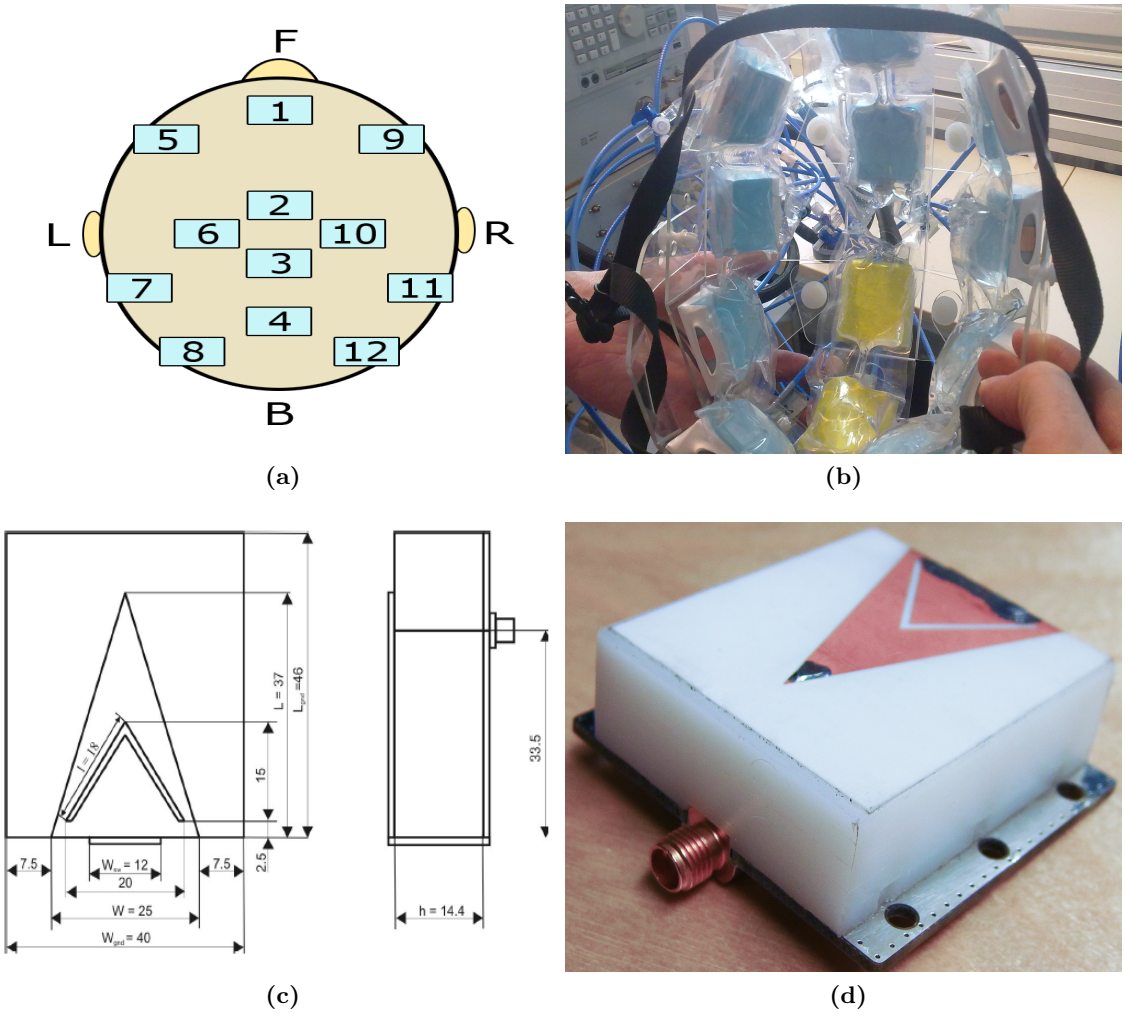

Figure 2.1: (a) Top view of MWH with antenna numbering. (b) MWH after assembling. (c) Top and side views of antenna with geometrical details [24]. (d) Photo of antenna.

Figure. 2.1 (c,d) shows the antenna used in the MWH, and geometrical details of this antenna. It is a triangular patch antenna which sends and receives signals in the frequency range of 0.1 to 3 GHz. The use of microstrip technology provides these antennas with excellent features like small size, light weight and low cost [24]. The antenna array in the MWH is sensitive enough to measure small changes in the brain [24].

2.1.2 Experimental setup at Chalmers

The experimental setup at Chalmers consisted of the programmable network analyzer (PNA, Agilent E8362B, Agilent Technlogies, Santa Clara, CA, United States), which transmitted and measured the microwave signals, a switching box (CXM/ 128-5-W) where 32 antennas could be connected, a dielectric probe kit (Agilent 85070E, Agilent Technlogies, Santa Clara, CA, United States) for measuring dielectric properties of phantom solutions, the MWH described above, a computer with all the necessary software installed, and the measurement object (Figure 2.2 (d)). The measurement time for one measurement was approximately 2 min, when 12 antennas were attached.

The dielectric probe kit was used to measure the dielectric properties of phantom solutions. The probe was connected to the PNA via the coaxial cable to port one. The measurements were performed using the already installed software which came with the kit. The dielectric probe kit was calibrated each time before it was used to measure the dielectric properties. The frequency range on which dielectric properties were measured could be selected in the software. The dielectric probe kit was mounted on a stand, which was very important for holding it in a stable position while measuring (Figure 2.2 (c)).

The computer used contained the Windows® XP based operating system. MATLAB® (version R2008b/R2011b, MathWorks Inc., Natick, MA, USA) installed on this computer was used to see the results of object measured and to save data for later processing. The PNA and switching box was controlled by software developed in-house.

2.1.3 Experimental setup at Medfield Diagnostics

The experimental setup at Medfield Diagnostics lab had the following main components: Vector network analyzer (VNA), the MWH described above, a personal computer and the object measured (see Figure 2.3).

VNA had a built in switching matrix and did not need a separate switching box. It was properly calibrated before use to decrease the noise level [6]. The calibration was performed by using a calibration kit, which was not as convenient as using the electronic switch box at Chalmers. The VNA had 12 ports. Software used to control the VNA was available in-house in LabVIEW™ (version 10.0, National Instruments, Austin, TX, USA) and Visual Studio® (version 2005, Microsoft, Redmond, WA, USA). The software provided many useful features required for experiments, and the measurement procedure was easier than at Chalmers. The measurement time for one measurement was approximately 1 min, when 12 antennas were attached. The operating system used was Windows® 7 (version 6.1 Service Pack 1, Microsoft, Redmond, WA, USA). Special

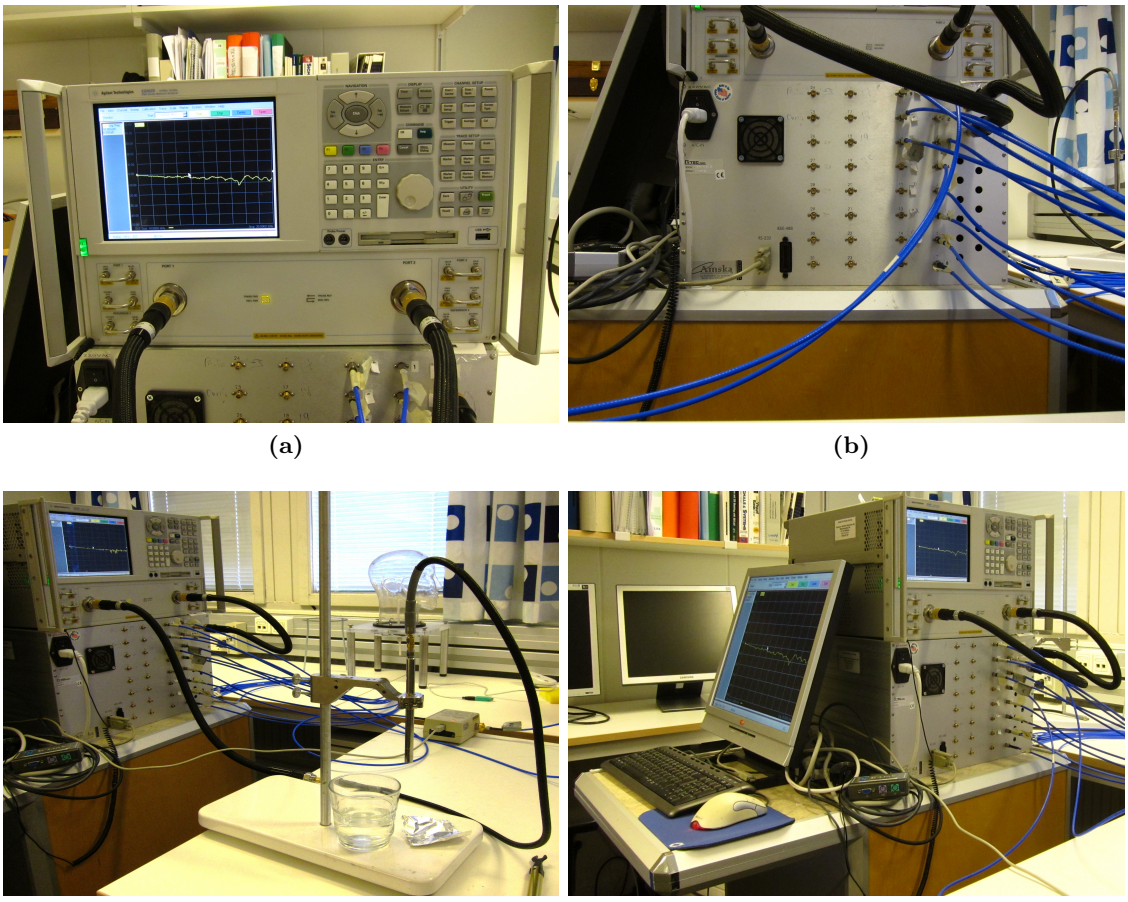

(a) **(b)**

(c) **(d)**

Figure 2.2: (a) Network analyzer. (b) Switching box. (c) Dielectric Probe kit. (d) Whole experimental setup at Chalmers University lab

care was taken to turn on the whole system well before $(40 - 45$ mins) performing any measurements at both labs, to suppress any possible warmup effects.

2.2 Phantom construction

A phantom is a tissue mimicking material which has certain properties in common to real human tissue. This study is based on comparing phantoms dielectric properties such as conductivity and permittivity to real human tissue. Phantoms are used to test a new medical product, before testing it on real humans [25].

Phantom construction was one of the main goals of this thesis and all measurements results depended upon this main step. There were many phantoms created during the thesis work, first in buckets and then an advanced phantom was created inside a human

cranium. Two types of phantom solutions were made, one which had similar dielectric properties as human grey matter in brain and the other having similar dielectric properties as human blood. Main steps in phantom construction were: preparing the solutions for the phantoms, measuring and comparing their dielectric properties and making solid phantoms from the solutions made.

2.2.1 Solution preparation

Phantom solutions were made according to the recipes in table 2.1. The measuring instruments used to measure the quantity of ingredients added were very simple and bought from supermarkets. Small quantities of formaldehyde solution (Formaldehyde solution 37 wt. % H_2O, Sigma aldrich, St. Louis, USA), around 3 mL per liter, were added to protect the phantoms against fungus.

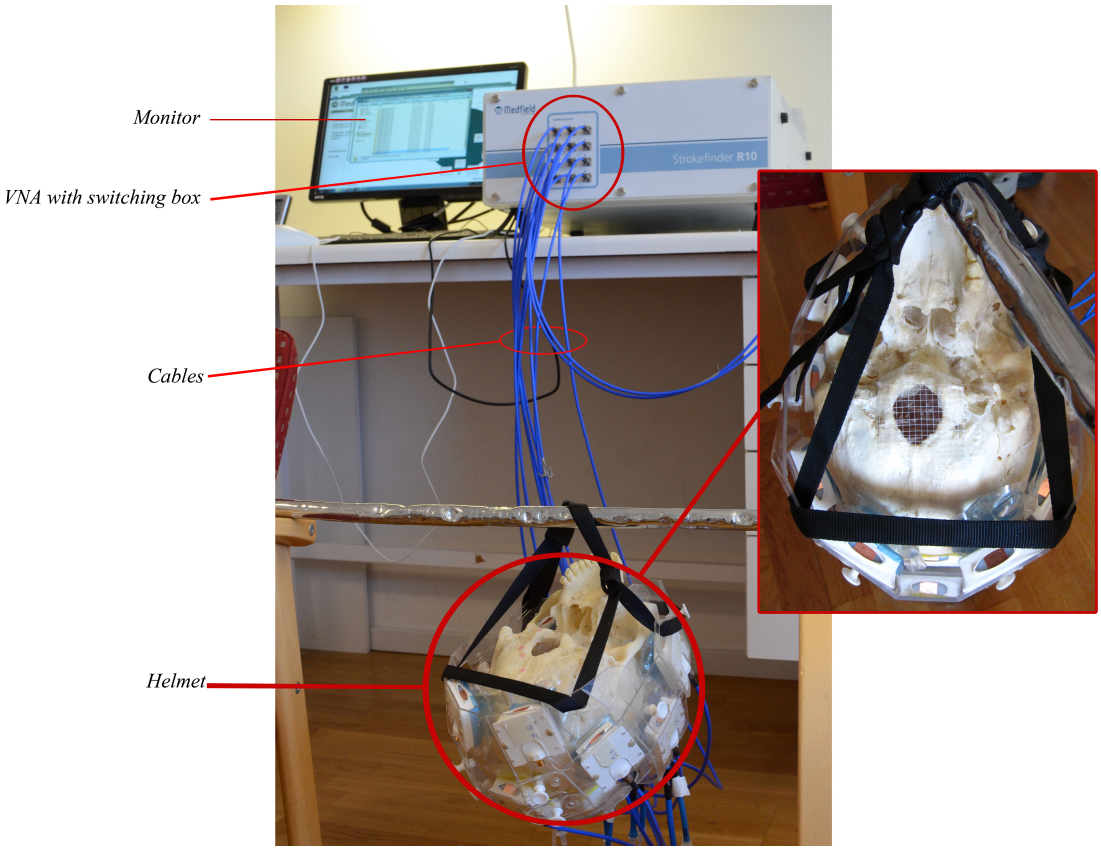

Figure 2.3: Experimental Setup at Medfield Diagnostics

(a)

Ingridents	Volume Percentage
Agar	5.8
Sugar	26
Salt	0.2
Water	68

(b)

Ingridents	Volume Percentage
Agar	3.9
Sugar	36
Salt	0.1
Water	60

Table 2.1: (a) Blood phantom recipe. (b) Grey matter phantom recipe.

2.2.2 Dielectric properties

Dielectric properties, the conductivity and permittivity values, of the phantom solutions were measured with the dielectric probe kit. The software gave the values of complex permittivity in the form of ε' (real part) and ε'' (imaginary part) [25]:

$$\varepsilon = \varepsilon' + i\varepsilon'' \tag{2.1}$$

Conductivity can be calculated as in eq. 2.2 [25],

$$\sigma = \omega\varepsilon_0\varepsilon'' \tag{2.2}$$

where, ε_0 is electric permittivity of free space and $\varepsilon_0 = 8.854 \times 10^{-12}$, ω is angular frequency and $\omega = 2\Pi f$. The results obtained were compared with [6] and [17].

2.2.3 Phantom construction process

After measuring the dielectric properties of both phantom solutions, agar (Agar fine powder, Sigma aldrich, St. Louis, USA) was added according to the recipe in Table 2.1, to make solid phantoms. Some red color (Rod hushallfarg, Dr. Oetker Sverige AB, Molndal, Sweden) was added to the bleeding phantom. The solution was heated and stirred until the temperature reached 70°C, and maintained above 70°C for 4–5 minutes, because otherwise it did not solidify well. The solution was poured into the bucket/human cranium, and it took approximately 30–60 min before it solidified at room temperature. In order to solidify it faster the container was sometimes put in a bath of cold water. The technique was similar for making both blood and gray matter phantom.

2.2.4 Phantom with bleeding

After making some initial tests to establish a good technique for making a phantom, efforts were made to make a phantom with a bleeding inside. Figure 2.4 shows some early tests of making a complete bleeding phantom in a bucket. Here, first blood phantom was made as in Figure 2.4 (b), then blood phantom was cut according to the desired size and shape. To be able to place the bleeding at a specific depth in the bucket, gray

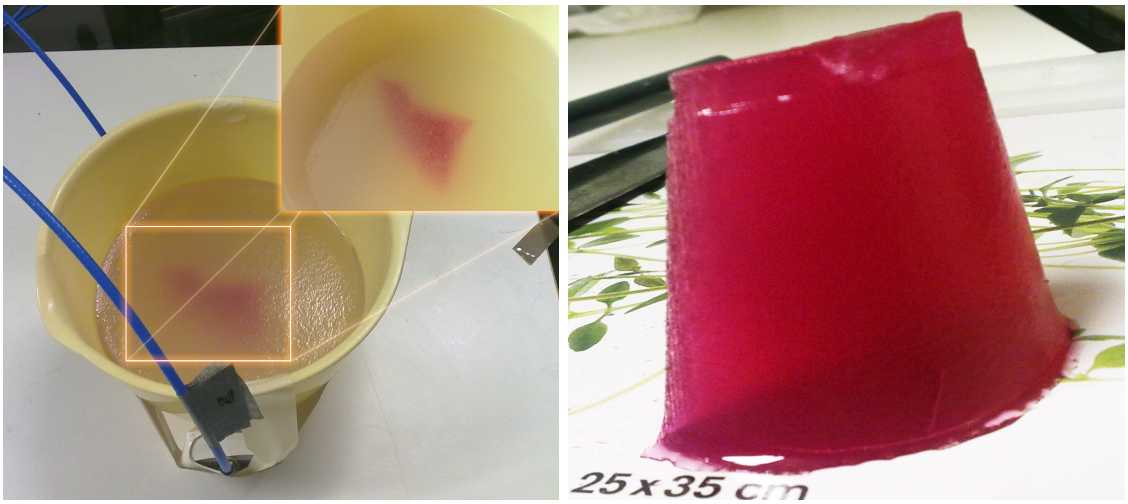

(a) **(b)**

Figure 2.4: (a) Showing the process of making bleeding phantom inside gray matter phantom and measuring on them. (b) Showing the already made blood phantom.

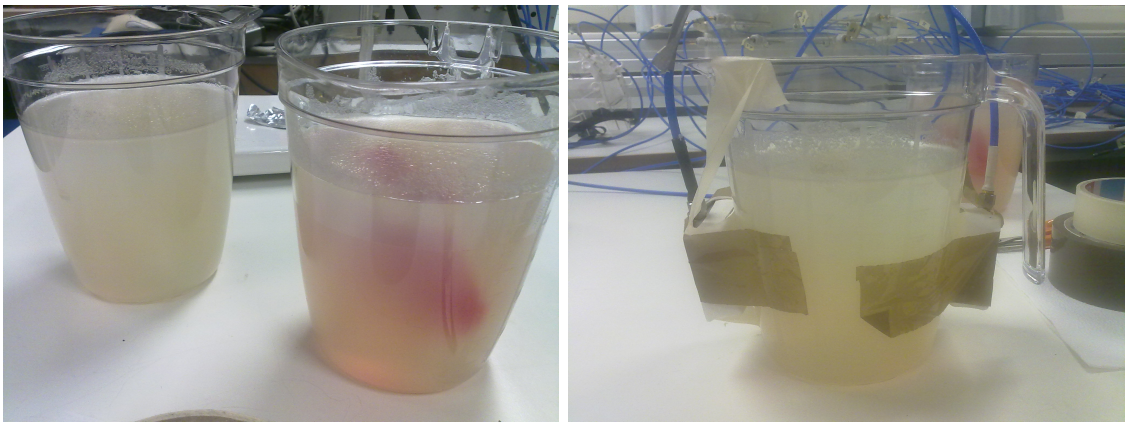

(a) **(b)**

Figure 2.5: (a) Shows two buckets, one without bleeding and one with bleeding. (b) Antennas attachment during measurements.

matter phantom solution was added in three layers. When the first layer had solidified the bleeding phantom was placed on top of it, and then the second layer was added, the purpose of this layer was to fixate the position of the bleeding. Finally, as the second layer turned solid, a third and final layer was added.

After these early tests, two phantoms in two buckets were made; these buckets were exactly similar in dimensions (see Figure. 2.5 (a)). One bucket contained phantom solution without bleeding and the other was with bleeding.

In the next step, four bucket measurements were made (Figure 2.6). One bucket contained phantom without bleeding, and the others contained different sizes of bleedings. The weights of the different sizes were 40, 60 and 90 grams.

(a) **(b)**

Figure 2.6: (a) Experimental setup used. (b) Shows four buckets, one without bleeding and other contains 40, 60 and 90 grams of bleeding.

2.2.5 Human cranium phantoms

A human cranium was used to make a more realistic phantom (see Figure. 2.7 (a)). There was only one human cranium available, so it was used repeatedly to make first without bleeding phantom and then different sizes of bleeding. Since the human cranium was cut in two pieces and there were naturally occurring holes in it, one challenge was to prevent the phantom solution from leaking out after filling the cranium (Figure 2.7 (a)). To cope with this leakage issue and holding the skull at a stable position, first a single layer of strong water proof tape was applied around the skull very carefully in small steps. Then the skull was tightly wrapped by plastic foil so that phantom solution stayed inside the plastic foil wrapping.

Figure. 2.7 (a-d) explains the process of making phantom inside human cranium. This protected human cranium against leakages was carefully placed in a bucket which helped in putting the skull in a stable position. Phantom substance was poured in from hole at the top of skull using a funnel until the cranium is completely filled (see Figure. 2.7 (c)). Then human cranium was further placed in a plastic bag and cold water was poured in the bucket from sides so phantom solidified quickly. The purpose of putting the skull in plastic bag was that no water may accidently flow in to the human cranium. When the phantom had solidified, the plastic foil and excessive phantom substance was removed. Figure 2.7 (d) shows how the phantom looked like after it had been solidified.

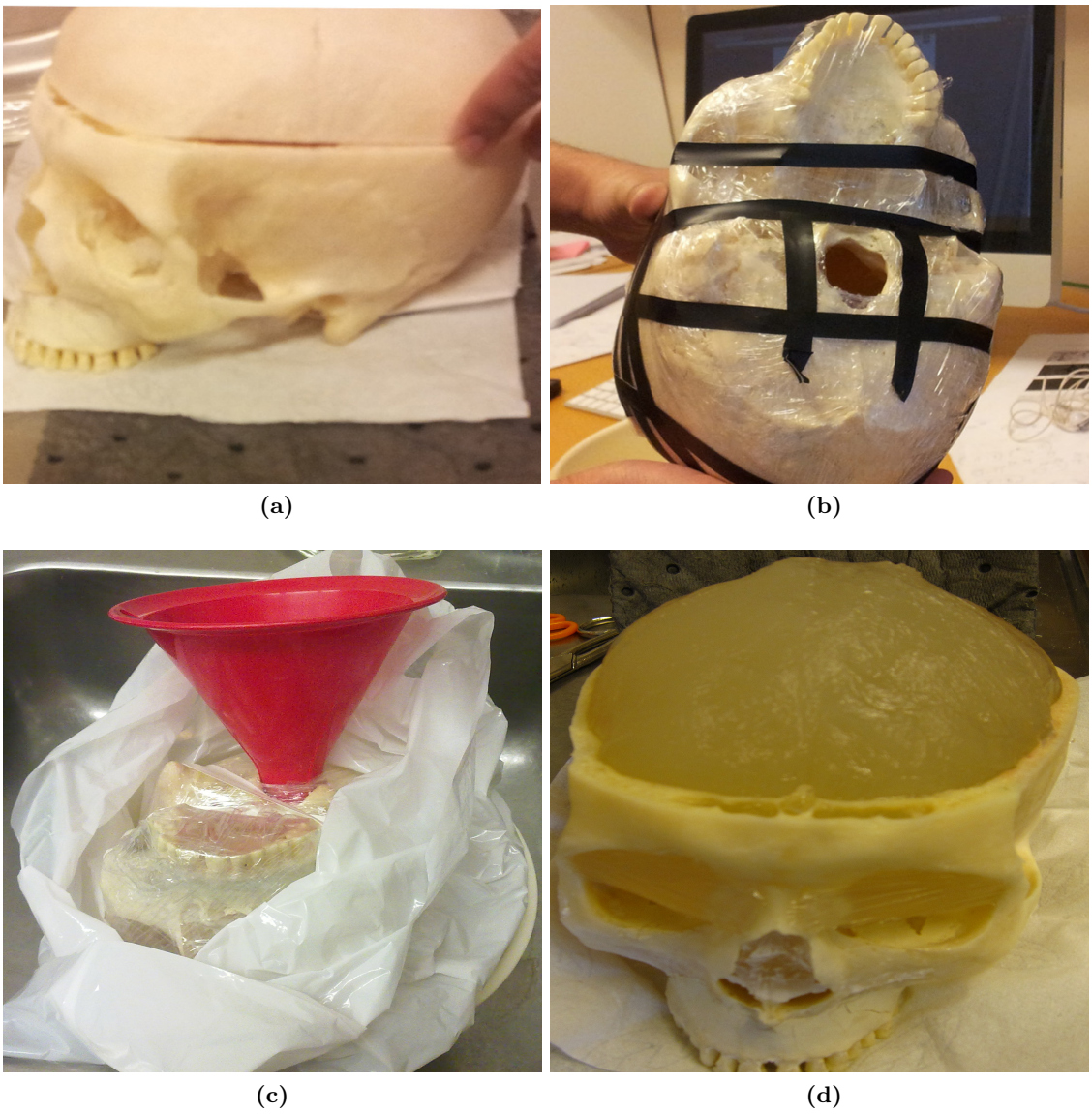

(a) **(b)**

(c) **(d)**

Figure 2.7: (a-d) Process of phantom making in human cranium

In this study it was tried to model SDH, Bullock et al. [5] mentioned that for acute SDH bleeding, a surgical removal is required if thickness exceeds 1 cm or a midline shift greater than 0.5 cm on CT scan. Ducruet et al [26] mentioned that SDH bleedings usually are like crescent-shaped. In order to test, whether MWT can detect bleeding of this size and shape, many experiments on phantoms were conducted to investigate whether there was any difference between phantom without bleeding and different sizes of bleedings. Efforts were made that bleeding introduced had the shapes and sizes according to findings mentioned above.

(a)

Ingridents	Volume Percentage
Agar	6
Sugar	26
Salt	0.2
Water	67.8

(b)

Ingridents	Volume Percentage
Agar	6
Sugar	36
Salt	0.1
Water	57.9

Table 2.2: (a) Blood phantom recipe. (b) Grey matter phantom recipe.

After making without bleeding phantom in human cranium, bleeding phantoms of sizes 40, 70 and 110 mL were introduced by cutting the same without bleeding phantom. The sizes of bleedings were chosen ranging from smallest i.e. 40 mL (width 0.5cm), which is under recommendation for surgery [5], to two sizes 70 mL (width 1cm) and 110 mL (width 1.5cm), which were above recommendation. Furthermore, concentration of agar was increased and water was decreased while preparing phantom solution to make a more solid phantom. The changes in the recipe can be seen in the table 2.2.

Bleedings were introduced in the following way, first the smallest bleeding was made, the skull was closed as described before. Next, the bleeding was removed, a larger bleeding was introduced and then measured, and so on.

The technique of making the bleeding phantom was different from the bucket experiments. The bleeding was created by first cutting away gray matter phantom using a scalpel, forming a realistic shape and size of the bleeding. Semi-liquid phantom was then poured at the bleeding site, carefully molded using the fingers to create the right shape. The skull was closed before the bleeding phantom had fully solidified, and turned upside down so the bleeding would be precisely shaped after the inside of the skull by the pressure, and left to fully solidify for about 30-45 mins. At first the smallest bleeding size of 40 mL was introduced followed by larger bleeding sizes of 70 mL and 110 mL respectively. To verify that bleeding visually looks satisfactory the upper part of the skull was removed once more and photographs were taken before the skull was sealed and measured. Figure. 2.8 (a) shows without bleeding phantom after it had been moulded and shaped according to recommendations for SDH in [5]. Figure. 2.8 (b, c) shows how phantom looks after introducing bleeding of 40 and 70 mL. Figure. 2.8 (d) shows the phantom with 110 mL bleeding after it has been removed from human cranium.

2.3 Experimental procedure

2.3.1 Two bucket and four buckets experiments

Two buckets experiment was performed at Chalmers University Lab. Two buckets were measured one by one, by attaching the same two antennas to buckets in random order (see Figure. 2.5 (b)). Ten measurements were performed in a randomized order. Four

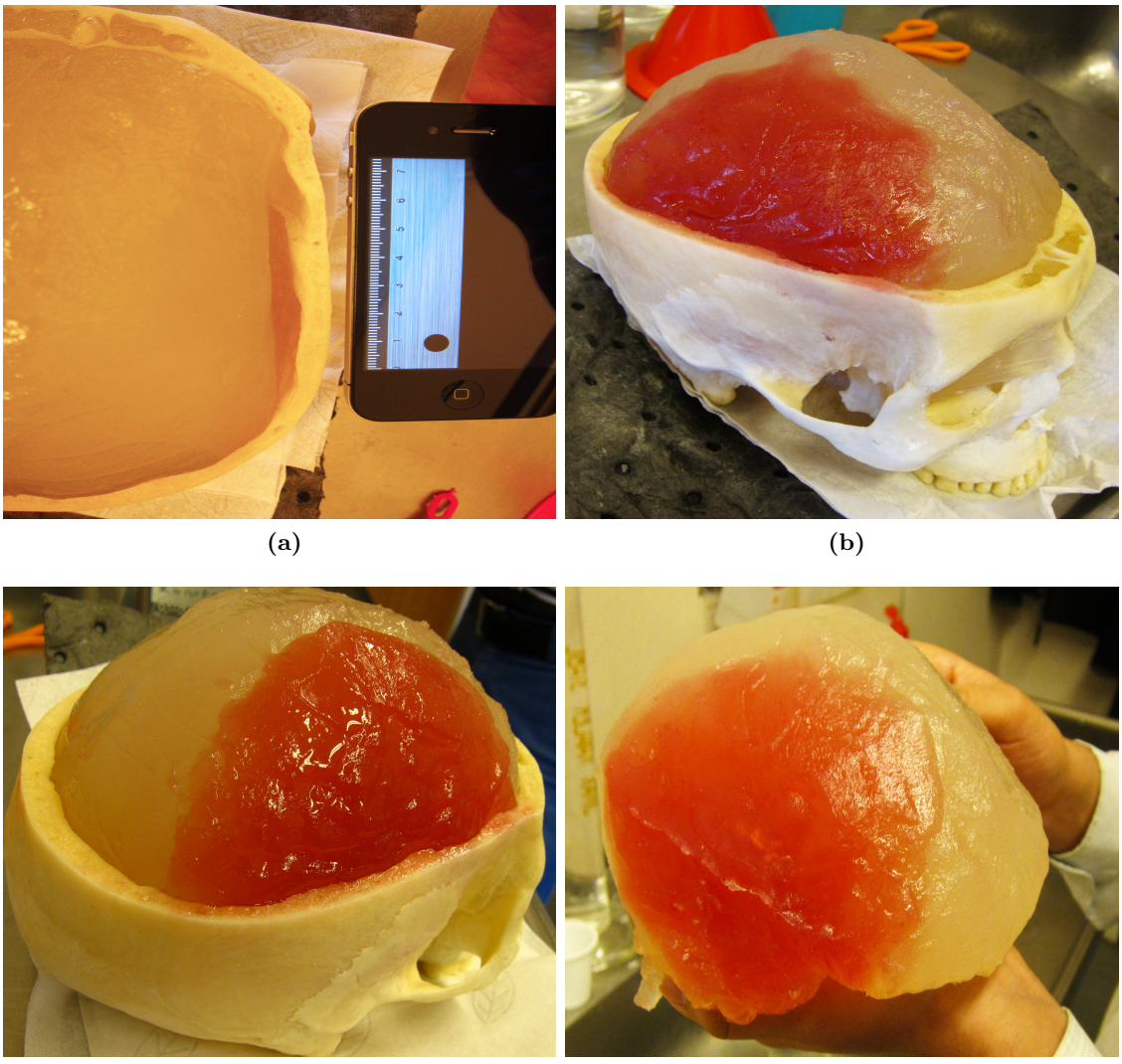

(a) **(b)**

(c) **(d)**

Figure 2.8: (a) Process of introducing bleeding in human cranium. (b, c) Phantom with 40 and 70 mL bleeding. (d) Phantom with 110 mL bleeding after removing from cranium.

buckets experiment was performed at Medfield Diagnostics and again ten measurements were made on each bucket in a randomized order. The difference between this experiment and the previous one was that antennas were not placed directly on the buckets but rather attached to fixed supports (Figure 2.6 b). Furthermore, water bags were attached to antennas for efficient coupling to the measurement object. This helped in applying the antennas at same angles and height to all buckets. This setup also improved the speed of performing the experiments comparing with two buckets experiment because in this way one just has to change buckets without need for applying tapes on antennas

correctly.

2.3.2 Human cranium experiments

Experiments on human cranium were performed at Medfield Diagnostics. Measurements were performed by the specially designed MWH, where not all 12 antennas were completely attached to the skull while measuring. Antennas number 2, 3, 4, 6, 7, 10, 11, were completely attached, 1, 5, 9, were partially attached and 8, 12 were not attached at all (Figure 2.1 (a)). Figure 2.3 shows the experimental setup. Measurements were performed in such a way that skull was moved 10 times deliberately in MWH after every 3rd measurement. In total 30 measurements (10 disturbances $\times$ 3 continuous measurements = 30) were performed. The reason for doing this was to mimic patient measurements where the MWH position on the head will vary from patient to patient and between different measurements on the same patient performed at different times. Same set of measurements were performed for different sizes of bleeding and without bleeding phantom and all measurements were completed within two days.

2.3.3 Interfering factors

To investigate different factors affecting the experimental setup e.g. apparatus movements, human interference and mobile signals, factors testing for both experimental setups at Chalmers and Medfield Diagnostics were performed.

The presence of a person around the experimental setup was investigated first. Measurements were performed on the measurement setup as shown in (Figure. 2.6 (b, c)). During measurements one volunteer was deliberately asked to stand near and away from measurement setup according to a randomized order. Second factor tested was to observe how mobile phone signals around the measurement setup affected the measurements results. Same measurement setup with mobile phone placed near it was used, while changing its status according to a random order from calling to offline mode. Third factor tested was to measure how cable movements during the measurements affect the measurement results. In this setup of measurements the cables were moved deliberately and rest of time they were kept still according to a random order. All above discussed factors were tested at Medfield Diagnostics.

Figure 2.9 explains the experimental setup used at Chalmers. Two factors were investigated there, i.e. mobile signals and apparatus movements. A volunteer wearing MWH was asked to hold a mobile phone near MWH. Here again mobile phone status was changed from calling to offline mode, according to a random order. This was done to test how mobile signals around the measurement setup affected the measurements results and compare these results with the tests performed at Medfield Diagnostics. In other type of factor testing, volunteer's chair was sometime shaken deliberately in random order to see how movements affect the measurements done.

Figure 2.9: Volunteer wearing helmet during fators testing at Chalmers University.

2.4 Data analysis

All the data analysis part was done in MATLAB®. A classification algorithm available in-house based on finding the minimum distance to the subspace bases which were calculated by singular value decomposition of the training data matrix for each class, were used to distinguish between bleeding and without bleeding and phantoms of different sizes and interfering factors. A brief overview and short description of algorithm is as follows.

2.4.1 Data processing and classification algorithm

Given C the total number of classes, let U_c be a subset containing data from class c, where $c \in \{1, \cdots, C\}$. Hence, $\forall\ x_{c,i} \in \mathrm{U}_c$, we have

$$\boldsymbol{x}_{c,i} = \boldsymbol{U}_c \boldsymbol{\alpha}_c(i) + \boldsymbol{e}_c \tag{2.3}$$

where, $\boldsymbol{U}_c$ is the subspace basis; vector $\boldsymbol{\alpha}_c(i)$ contains the weights of the basis vectors and $\boldsymbol{e}_c$ is white noise.

The distance from the data $\boldsymbol{x}_{c,i}$ to the basis $\boldsymbol{U}_c$ is computed as:

$$d_c(\boldsymbol{x}_i) = \left\|\boldsymbol{x}_i - \boldsymbol{U}_c\boldsymbol{U}_c^T\boldsymbol{x}_i\right\|_2 \tag{2.4}$$

Therefore, the criterion for classification is the smallest distance $d_c(\boldsymbol{x}_i)$, $\forall$ c.

2.4.2 Classification algorithm

The classification algorithm is as follows:

Algorithm 1 Classification algorithm ($c \in \{1,2,\cdots,C\}$):

- Pre-process the raw data to produce $\boldsymbol{x}_i$;
- Construct the measurement matrix $\boldsymbol{X}_c$ using the training data from class c:
$\boldsymbol{X}_c = \left[\boldsymbol{x}_{c,1},\cdots,\boldsymbol{x}_{c,N_c}\right]$;
- Calculate the basis $\boldsymbol{U}_c = \{\boldsymbol{u}_{c,k}\}$ for each class by Singular Value Decomposition (SVD):
$\left[\boldsymbol{U}_c,\boldsymbol{S}_c,\boldsymbol{V}_c\right] = SVD(\boldsymbol{X}_c,0)$;
- Compute the distance $d_c(\boldsymbol{x}_i)$:
$d_c(\boldsymbol{x}_i) = \left\|\boldsymbol{x}_i - \boldsymbol{U}_c\boldsymbol{U}_c^T\boldsymbol{x}_i\right\|_2$;
- Classify $\hat{c}_i$ by finding the smallest distance:
$\hat{c}_i = \arg\ \min_c\ d_c^2(\boldsymbol{x}_i)$.

Data pre-processing includes taking the logarithm of the raw S parameters and normalization of each channel to guarantee the equivalent contribution.

2.4.3 Application of algorithm

Data obtained was organized in classes (as class A, B, C, D....) on the basis of available data. The result was obtained by computing the distances from basis signal to all the subspaces simultaneously as explained above. Leave-one-out approach was used to compute the basis vector according to which each time sample which need to be classified was not included in the subspace basis.

In factors testing analysis, the difference between the distances (projection errors) form a signal to the two subspaces are calculated simultaneously i.e. $y = d_{x\to A1} - d_{x\to A2}$ where $x \to A_i$ means the signal projected on the subspace A_i, i = 1,2, and d means the distance.

3

Results

In this chapter results obtained from the experiments performed shall be presented i.e. dielectric properties measurements, two and four buckets experiments, human cranium experiments and interfering factors testing. Here only those plots for raw data measured from experimental setup are shown where a trend was seen visually without applying classification algorithm.

3.1 Dielectric properties measurements

In this section, results for the dielectric properties of the blood and grey matter phantom solution are shown. Figure 3.1 (a-d) shows the average permittivity and conductivity values of blood and grey matter phantom solution. Average is taken over 4 measurements for blood solution and 8 measurements for grey matter solution. The results obtained were in good agreement with Krishnan 2011 [6] and Gabriel et al., 1996 [17].

Figure. 3.2 and 3.3 shows the comparison of average permittivity and conductivity with standard deviation of blood vs. grey matter phantom solutions. These results show that there is a clear difference between dielectric properties of blood and grey matter phantom.

3.2 Results from two buckets experiment

Results from two buckets experiments are shown in Figure. 3.4 (a, b). These results show that we cannot differentiate between without bleeding and bleeding buckets.

3.3 Results from four buckets experiment

Figure. 3.5 and 3.6 demonstrates the raw measured data obtained from measurement setup, here average amplitude of 10 measurements for reflection and transmission co-

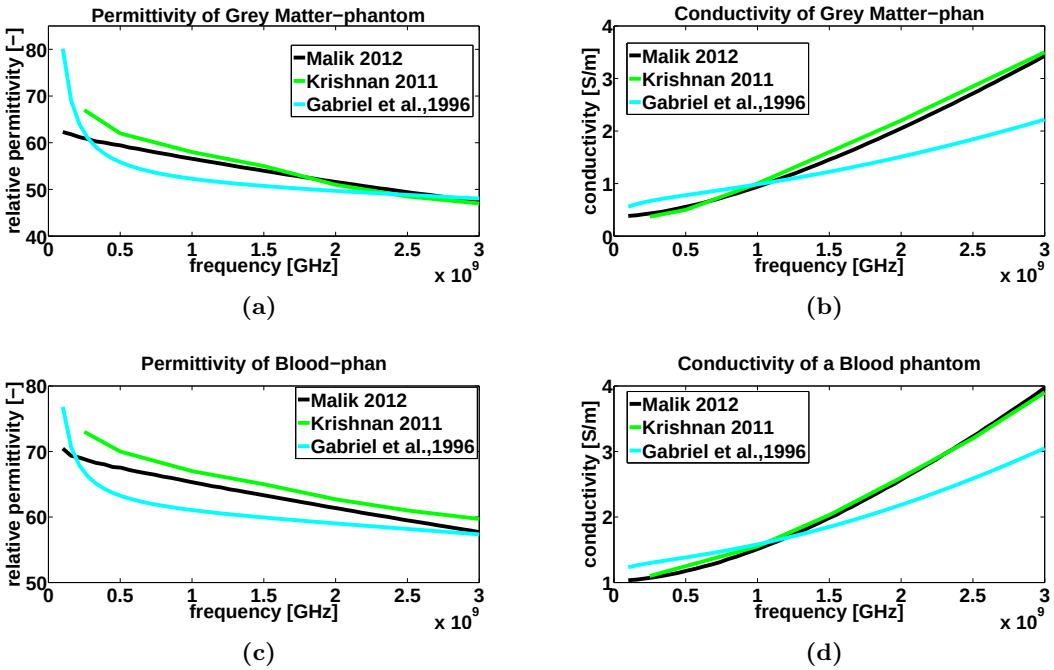

Figure 3.1: (a-d) Average Permittivity and conductivity of blood (n=4) and grey matter phantom (n=8) comparing with [6] and [17].

efficients are shown at certain frequencies. The average amplitude is shown only at those frequencies where a trend can be seen visually between no bleedings and bleeding phantoms. Without bleeding phantoms are different in amplitude in reflection and transmission signal compared to other bleeding phantoms at certain frequencies. Figure. 3.7 and 3.8 shows the mean amplitude calculated for 10 measurements, which shows again that mean amplitude of without bleeding phantom is different from bleeding phantom.

Figure. 3.9 shows the results obtained from the classification algorithm. Figure. 3.9 (a) shows that we can differentiate between without bleeding and bleeding buckets if we train our basis vector according to 0g bleeding. Figure. 3.9 (b) shows that we can differentiate correctly up to 70% between 40g bleeding buckets and other buckets if we train our basis vector according to 40g bleeding. Similarly, correctness is 80% and 60% if we take as 60g and 90g bleeding buckets as basis set (see Figure. 3.9 (c, d)).

3.4 Results from human cranium experiments

Figure. 3.10 and 3.12 shows the results of transmission signal measured at certain frequencies, where signal is transmitted from antenna number 7 to 10 and 7 to 11. The reason for picking these antennas combination was because of the placement of bleeding with respect to antennas (see Figure. 4.1 (a, b)). Figure. 3.11 and 3.13 shows the mean amplitude of transmission signal of certain antenna combinations. A difference

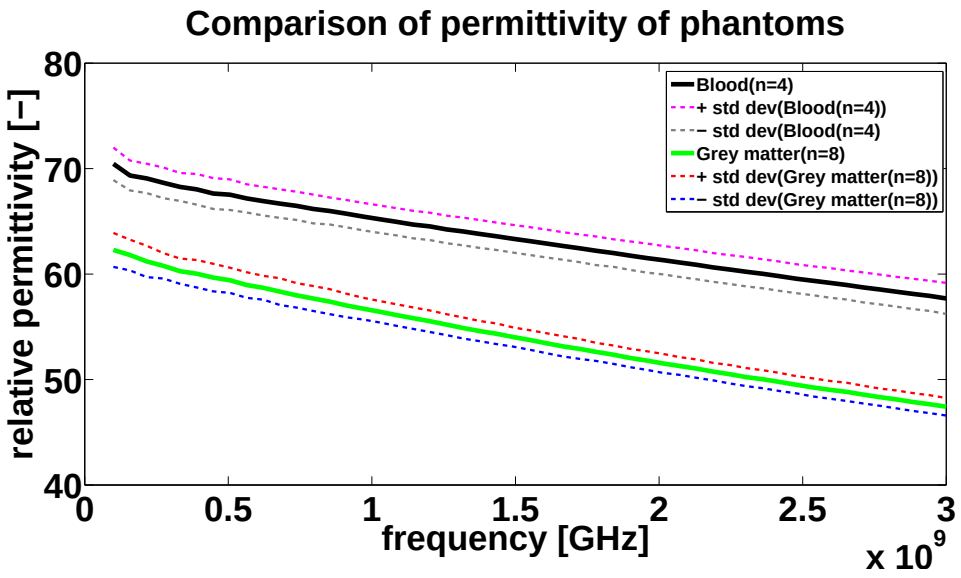

Figure 3.2: Comparison of average permittivity with standard deviation of blood (n=4) vs. grey matter phantom (n=8).

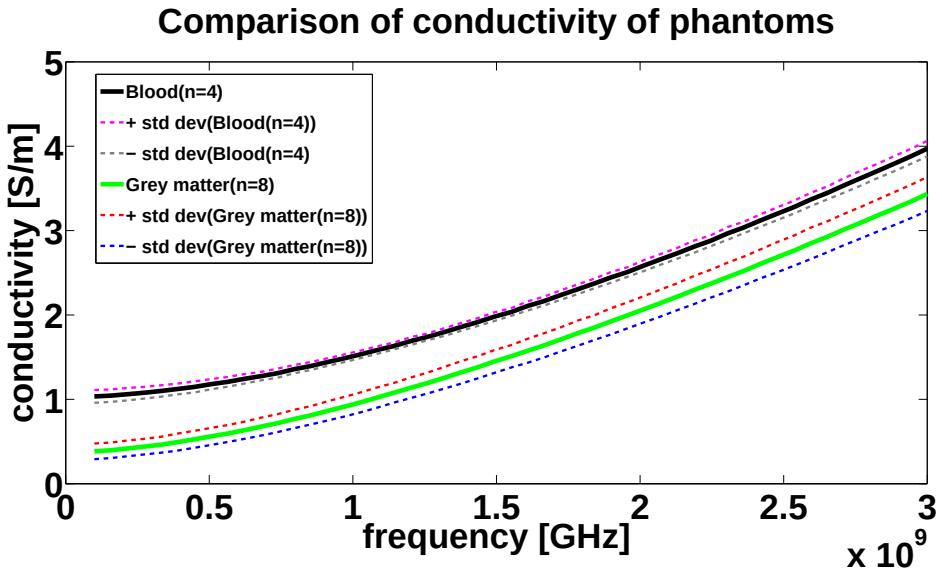

Figure 3.3: Comparison of average conductivity with standard deviation of blood (n=4) vs. grey matter phantom (n=8).

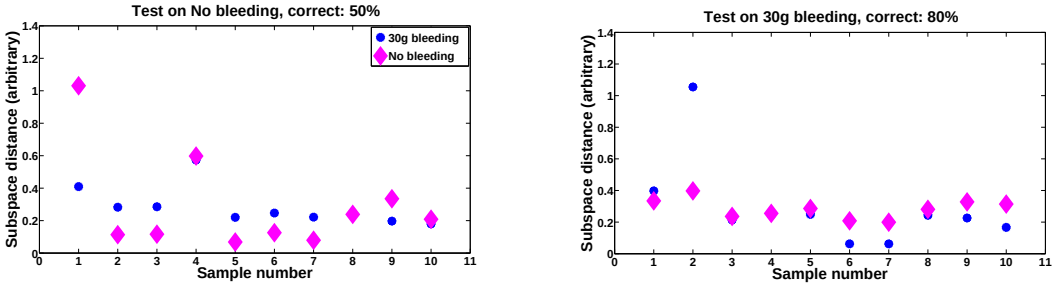

(a) (b)

Figure 3.4: (a-b) Classification algorithm results from two buckets experiment.

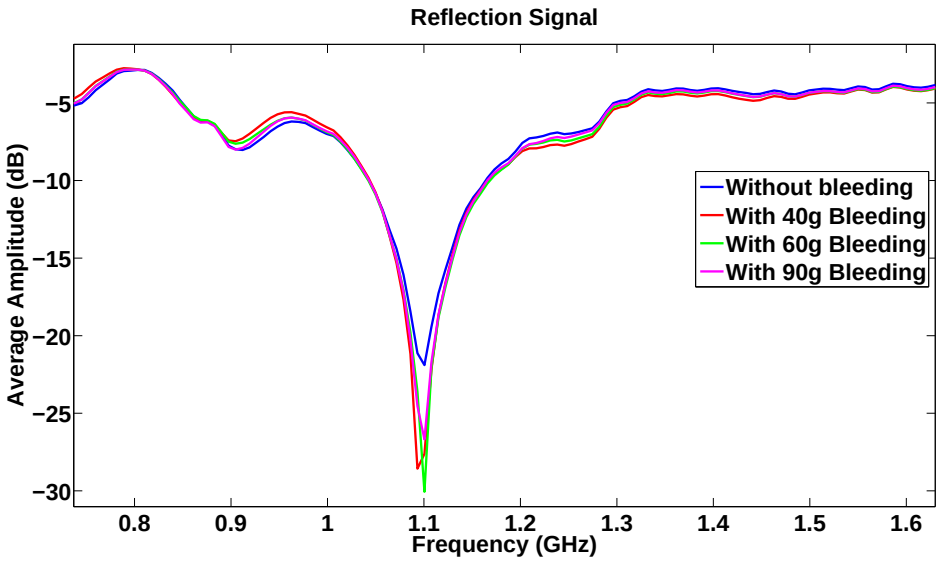

Figure 3.5: Reflection Signal for four buckets experiments (n=10).

between mean amplitude of without bleeding and bleeding phantom is found, following approximately same trend as in four bucket measurements.

Figure. 3.14, shows the results obtained from classification algorithm used for human skull experiments. These results were formulated by considering measurements from completely attached and partially attached antennas. Here, no matter which class of different cases we use to train our basis vector, we can differentiate correctly up to 100% between without bleeding and different sizes of bleedings phantoms. Therefore, we can not only differentiate between non bleeding and bleeding but also between different sizes of bleedings.

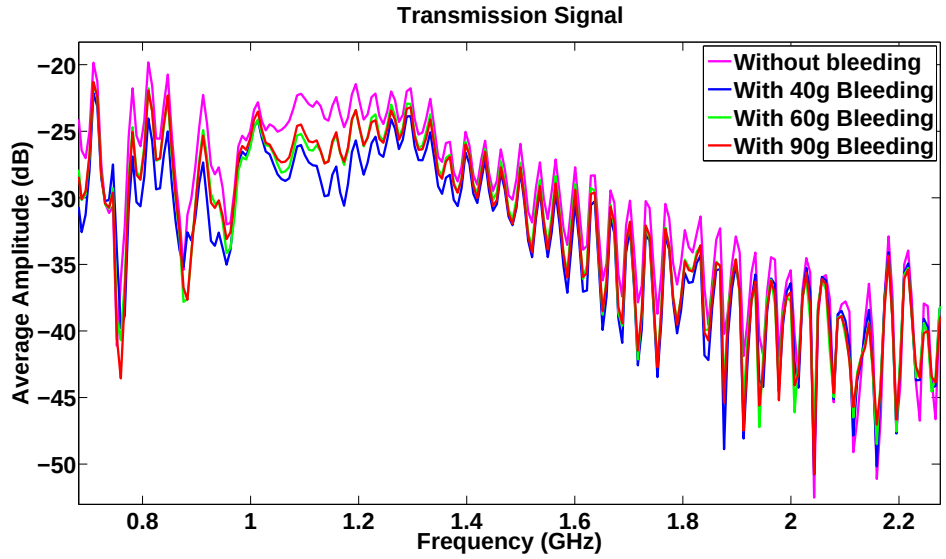

Figure 3.6: Transmission Signal for four buckets experiments (n=10).

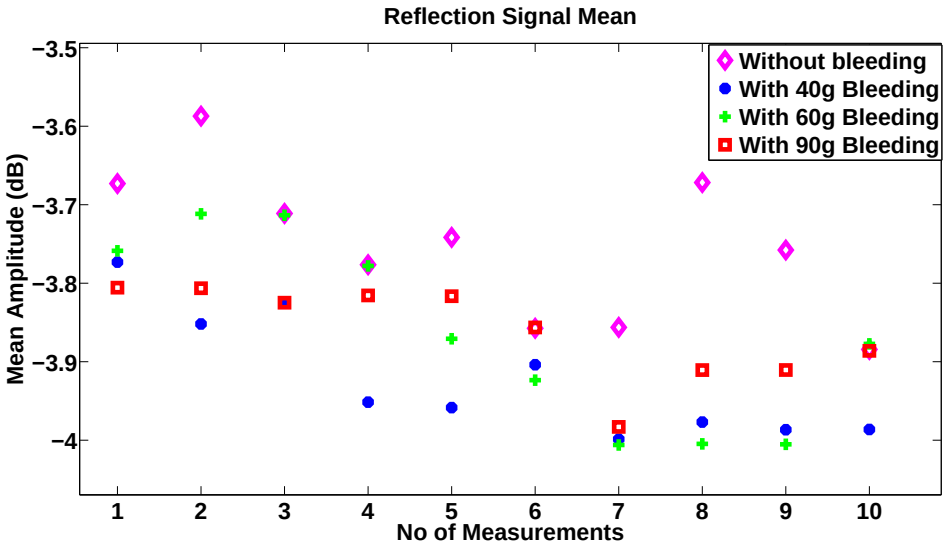

Figure 3.7: Reflection Signal mean for four buckets experiments (n=10).

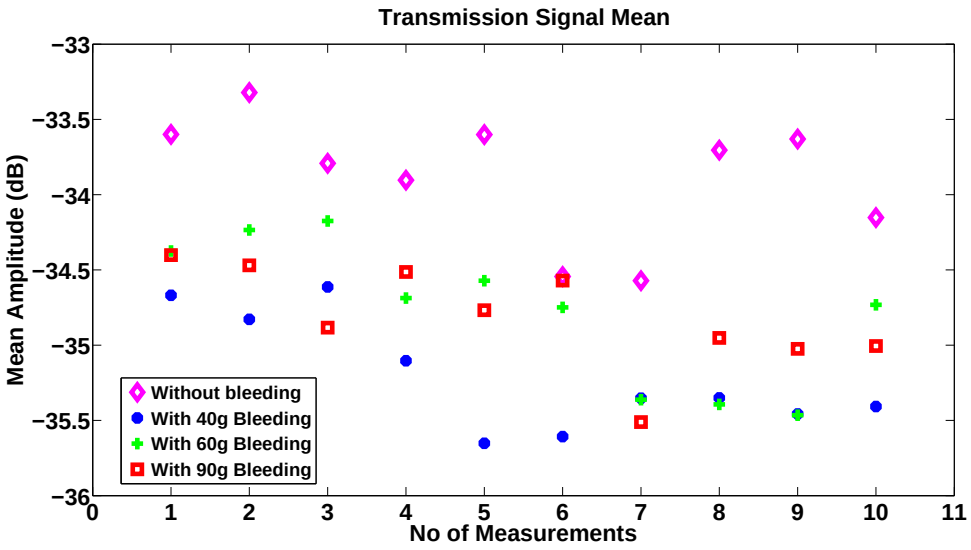

Figure 3.8: Transmission Signal mean for four buckets experiments (n=10).

3.5 Factors testing at Medfield Diagnostics

Figure 3.15 and 3.16 (a, b) shows the results of classification algorithm from potential interfering factors measurements. Figure 3.15 shows that signals are clearly separated with the factor of human interference.

Figure 3.16 (a) shows that there is no clear effect when cables are moved from still postition. However, in Figure 3.16 (b) a trend in difference between two measurements can be obseved.

3.6 Factors testing at Chalmers University lab

Figure 3.17 (a) shows that there is no clear effect when chair was shaken or not hence chair shaking during measurements seems to have no significant effect. Figure 3.17 (b), shows that mobile phone signal has some effect on experimental setup.

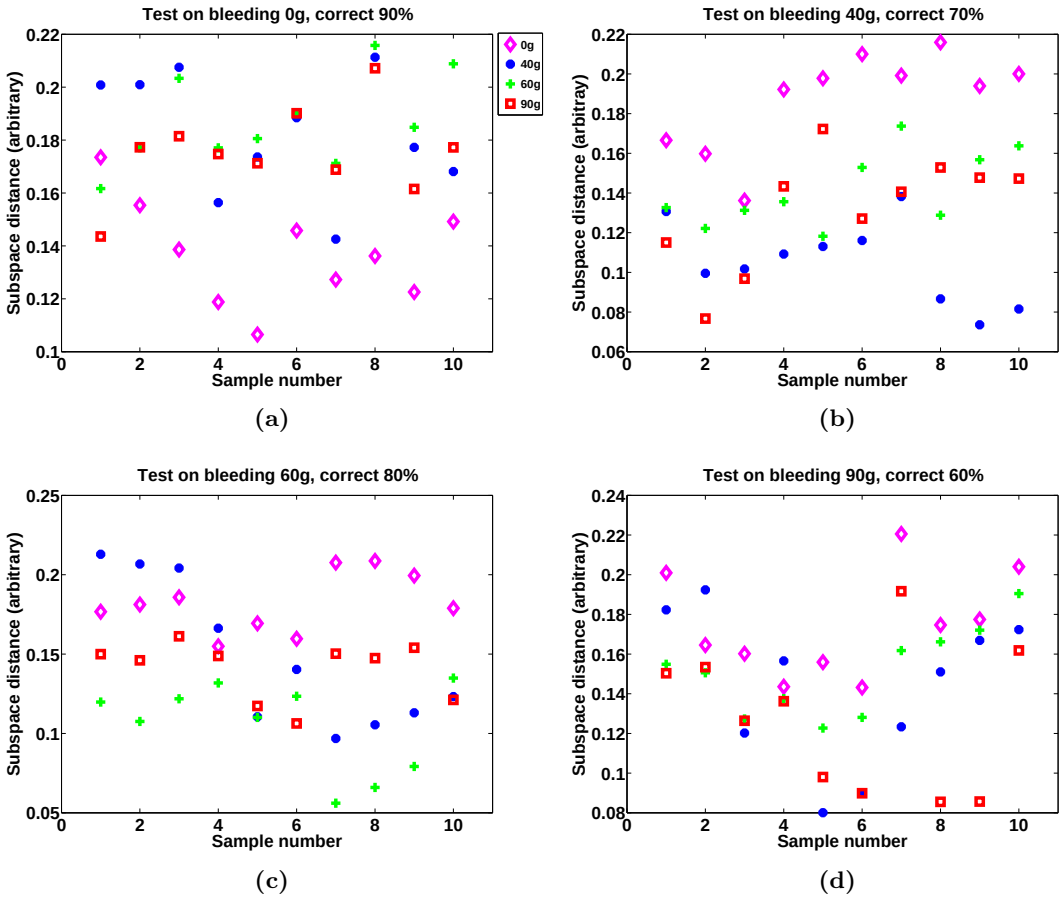

Figure 3.9: (a-d) Classification algorithm results from four buckets experiment.

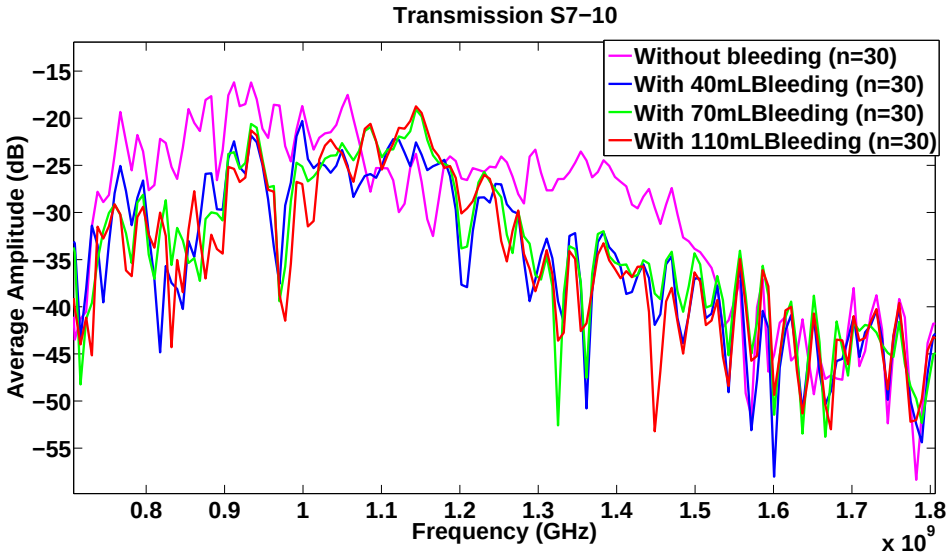

Figure 3.10: Transmission Signal S7-10 for human cranium experiments (n=30).

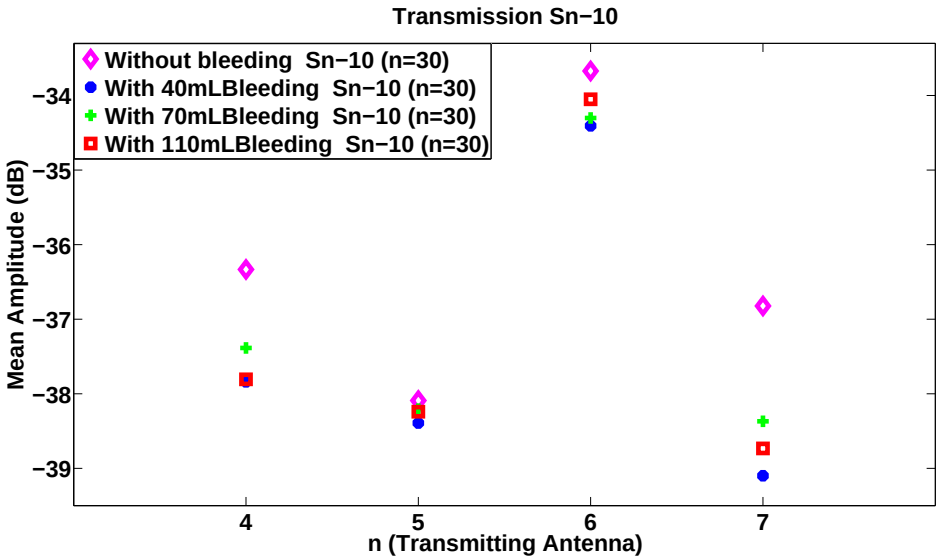

Figure 3.11: Transmission Signal mean for Sn-10 for human cranium experiments (where n=transmitting anttenas=4, 5, 6 and 7. 10 is receiving antenna).

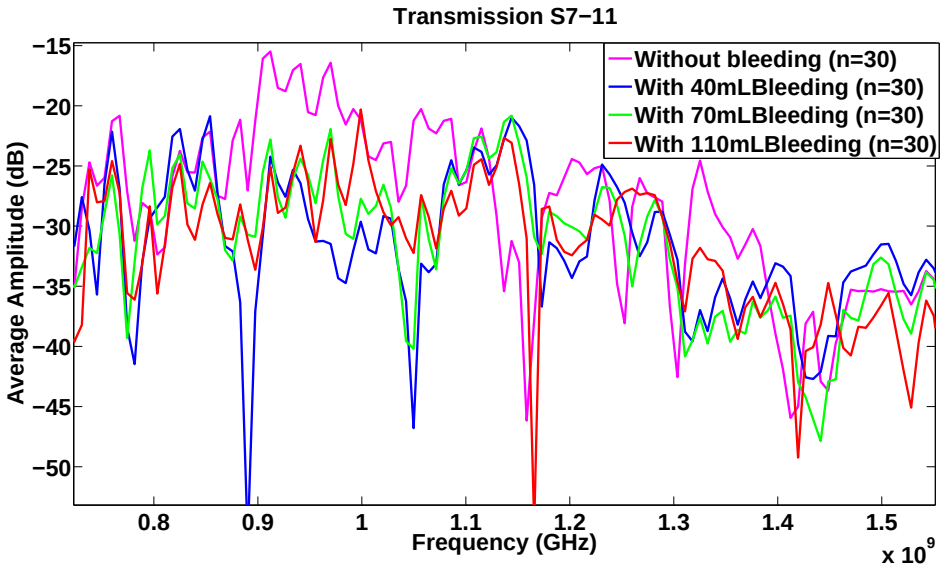

Figure 3.12: Transmission Signal S7-11 for human cranium experiments (n=30).

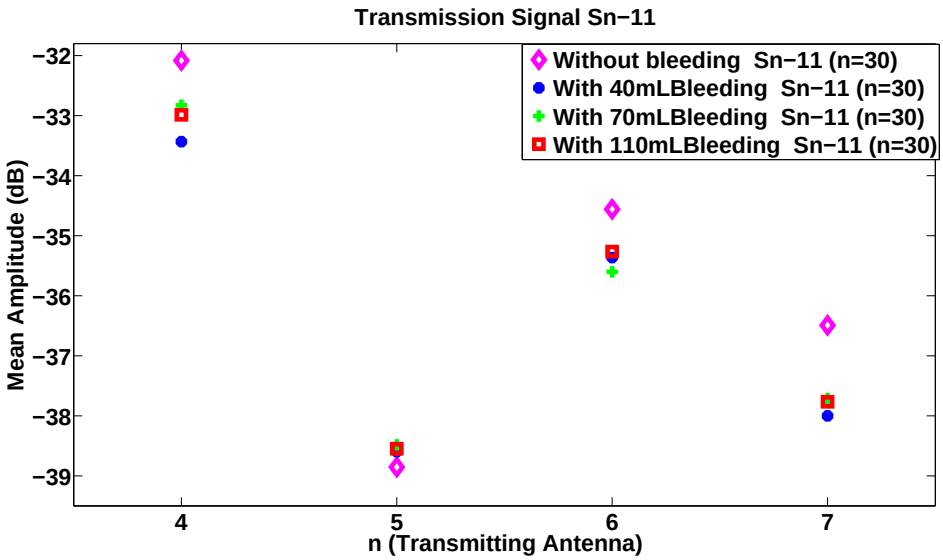

Figure 3.13: Transmission Signal mean for Sn-11 for human cranium experiments (where n=transmitting anttenas=4, 5, 6 and 7. 11 is receiving antenna).

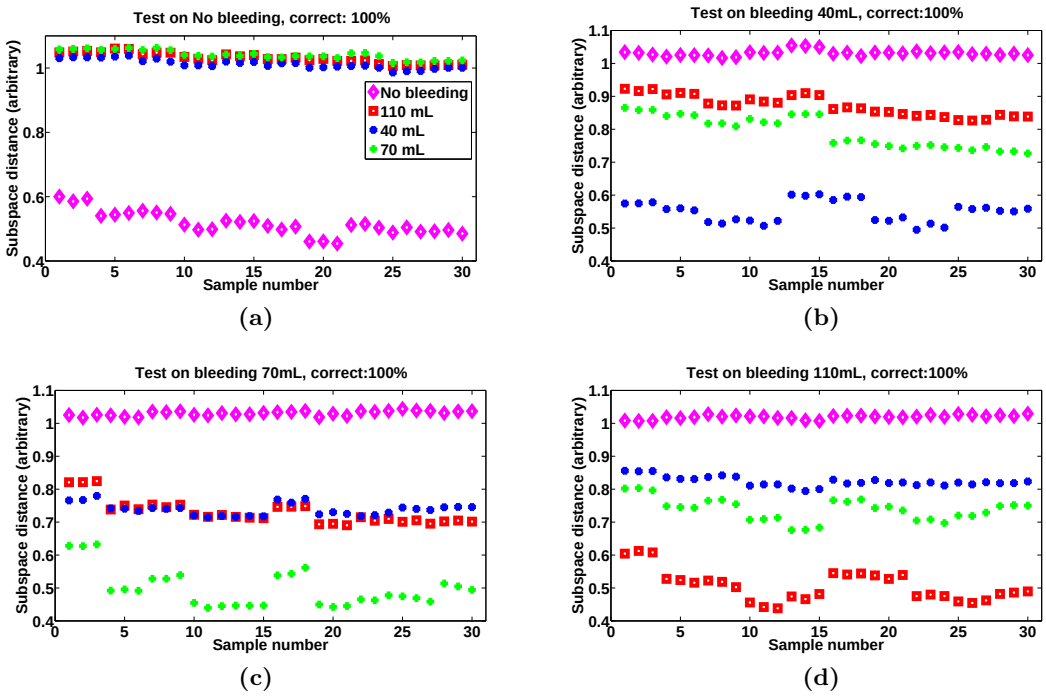

Figure 3.14: (a-d) Classification algorithm results from human cranium experiment

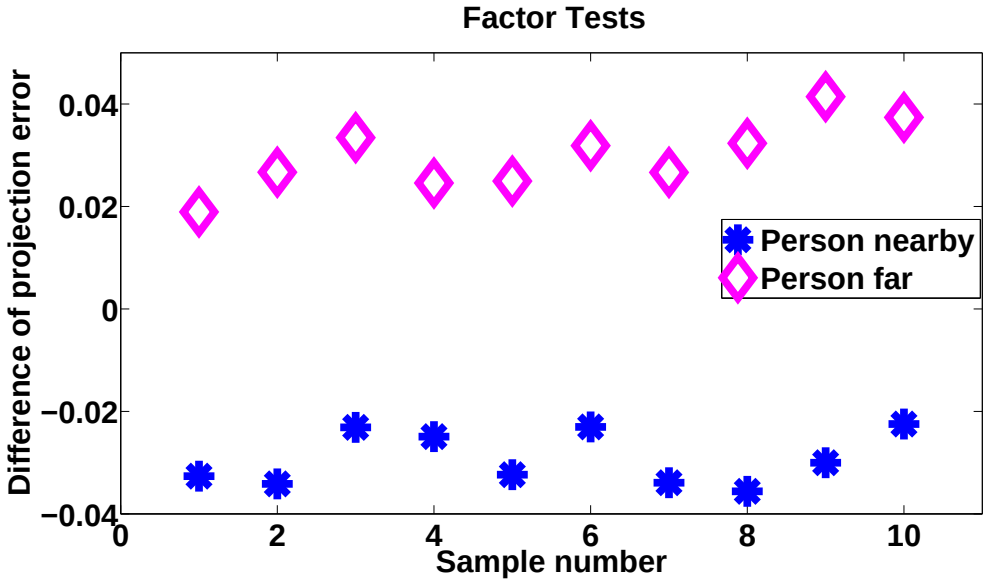

Figure 3.15: Results of effects of person standing near/away during measurements

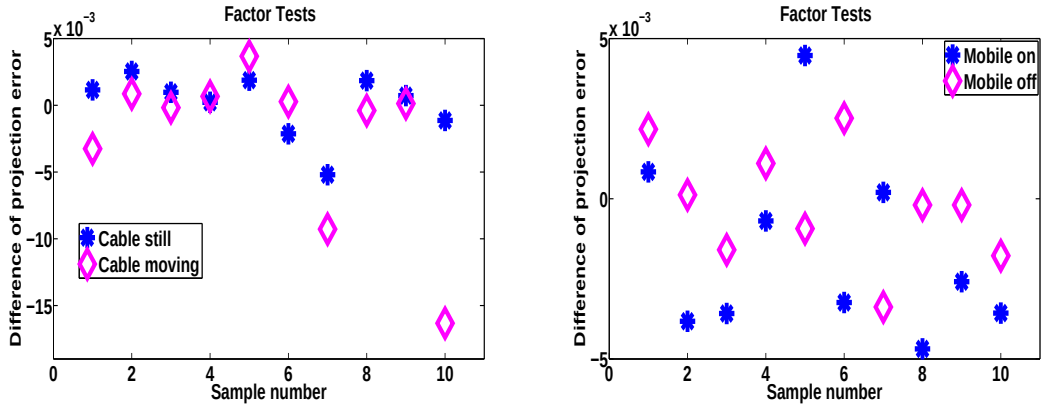

(a) (b)

Figure 3.16: (a) Cable still and moving results.(b) Mobile on/off results

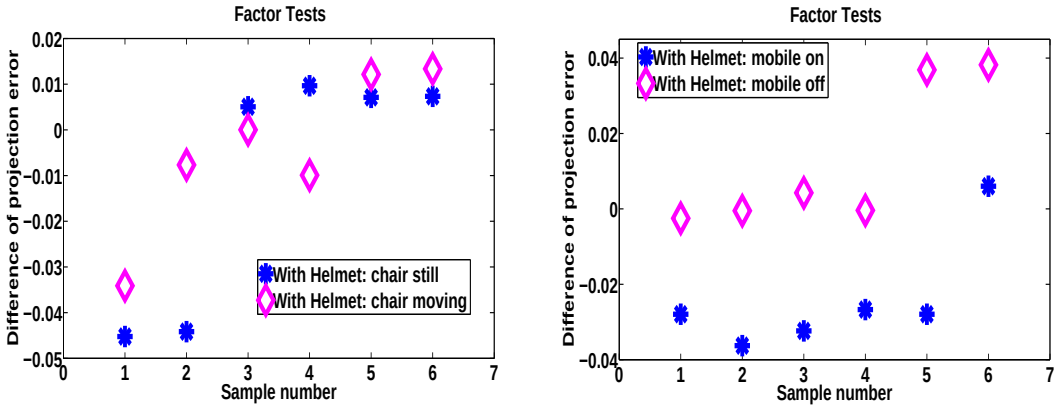

(a) (b)

Figure 3.17: (a) Chair still vs chair moving results. (b) Mobile on/off results

4

Discussion

4.1 Materials and methods

- Difficulties were faced during MWH construction and handling of MWH during measurement process. These were mainly due to some design problems in MWH i.e. placement of antennas, putting cables on and off, placing water bags at right positions and filling them with water etc.
- Care has to be taken while mixing the ingredients in section 2.2.1, so that they were properly measured and mixed according to recipe.
- It is important to note while measuring dielectric properties in section 2.2.2, that there should be no air bubble left on probe which could potentially introduce errors during measurements.
- In section 2.2.3, it is important to control the solutions temperature so that it is not over heated and that bubbles are left in phantom solution. Furthermore, while heating solutions proper stirring at slower pace must be done which will not only help in solidifying phantom uniformly, but also help in minimizing air bubbles in phantom which can result from fast stirring.
- In section 2.2.4, the purpose of making phantom in three layers was to overcome the air bubbles which can arise if one tries to introduce the bleeding after making the solid grey matter phantom. Furthermore, it made it easier to control the position of bleeding inside gray matter phantom. The size, shape and placement of bleeding is all dependent upon which bleeding you are modeling and can easily be controlled by the method presented in this thesis.
- In section 2.2.5, it is important that after heating solution for bleeding phantom let it solidify and when it is about to turn solid then place it on already molded

phantom with care. The size and shape of bleeding was an important measure to consider while introducing bleeding phantom in human cranium experiments. The size of bleeding phantom for human cranium experiments were measured by Archimedes' principle. The process of shaping bleeding phantom was difficult to control and should be done at right time i.e. when bleeding is about to turn solid.

- It is important to measure on newly made phantoms, otherwise, phantom lose water and contracts with time, which causes air gaps between the surface of phantom and the object containing phantom.
- It is good to have a stable experimental setup before measurements this will help in performing measurements efficiently.

4.2 Dielectric properties measurements results

Dielectric properties vary with addition or change in concentration of ingredients in recipe. Gund et al [25] has mentioned how dielectric properties changes with the change in concentration of different ingredients. The average and standard deviation plots showed that solutions for phantom making process have dielectric properties which do not vary much and are close to recommendations.

4.3 Two buckets experiments

The results in section 3.2 illustrates that the classifier was unable to differentiate between bleeding and non-bleeding phantoms. Moreover, we did a visual inspection of raw data to find some interesting trend or relation, but unfortunately the raw data did not showed any correlation and thus the results were excluded. The reasons for this behavior was due to small size of bleeding, some mistakes in phantom construction or solution making process, only two antenna used and unstable experimental setup.

4.4 Four buckets experiments

As shown in section 3.3, visual observation of raw data in the form of transmission and reflection coefficients showed some trends which was further confirmed in mean amplitude plots, where without bleeding phantom's amplitude is different from bleeding phantoms consistently during 10 measurements.

The classification algorithm was able to correctly differentiate between bleeding and without bleeding phantom up to 90% correctness. Therefore, these results were quite promising for further preparation of more realistic phantom in human cranium. Furthermore, in these experiments only two antennas were involved, where as in human cranium experiments more antennas were used which can further improve the results as in [27]. However, process of making phantom was more challenging in human cranium.

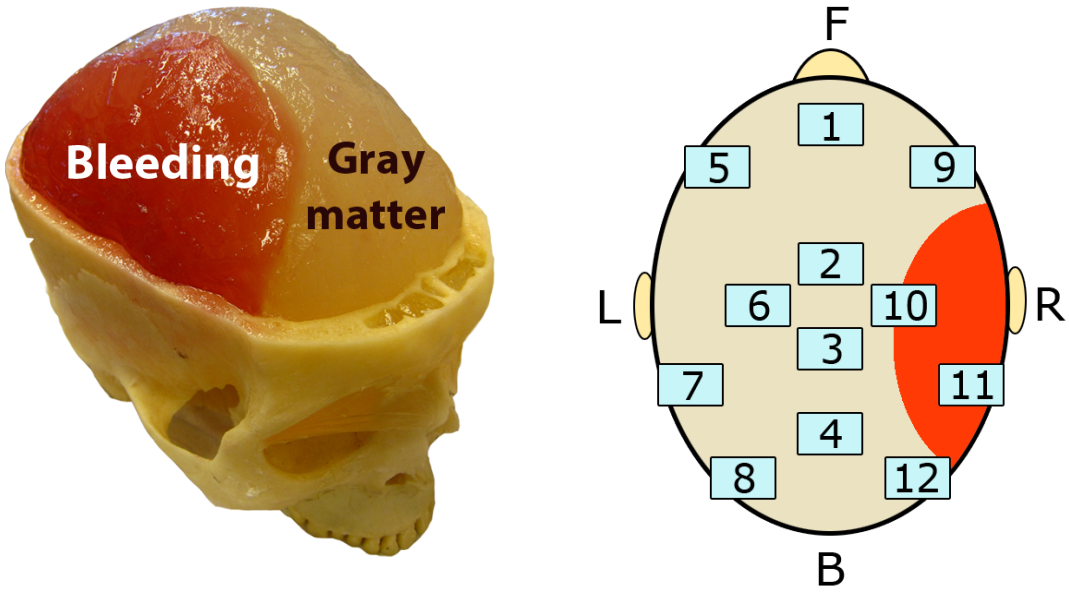

(a) (b)

Figure 4.1: (a) Showing the placement of bleeding in human cranium. (b) Showing placement of bleeding with respect to antennas.

4.5 Human cranium experiments

Visual observation of raw data in human cranium experiments also showed some similar trends as discussed above. Here again mean amplitude plots for transmission signal with different combination of antennas showed that without bleeding phantom's amplitude is different from bleeding phantoms consistently. Reflection signal was also studied but it did not show any trends, therefore, results for that are not presented. The reason why these antenna combinations have shown some trends could be because transmitting antennas number 4, 5, 6 and 7 are in good angles to receiving antennas number 10 and 11 in MWH. Therefore they can transmit signals perpendicularly to bleeding in comparison to others (see Figure. 4.1 (a, b)) [27].

Classification algorithm results showed in section 3.4, demonstrate that MWT has high potential for detecting bleedings of different sizes both under and above recommendations for surgery in SDH. Furthermore, there is a trend between different bleeding sizes which is as a measure of distance from the basis class. This result is very useful to carry out further testing of MWT for other types of bleedings.

4.6 Interfering factors testing

In section 3.5, it has been shown that person standing near experimental setup have significant effect on measurements results compared to other factors tested. However, it might depend on the particular setup, relative position of the person, size of object etc. Similarly mobile phone signals seems to have effect at Chalmers University Lab experimental setup however this effect was not clear at Medfield Diagnostics setup. Therefore, how strong signals effect the measuring results needs to be reviewed. The movements of parts of experimental setup seems to have very little impact on the measurements as compared to other factors results because no prominent effect has been seen at both labs. This result is quite promising for the portability of MWT in future and shows that MWT can be placed in ambulances in future. However, it is needed to be tested that can bleeding still be detected in the presence or absence of these factors and how strong influence of these factors restricts the MWT to detect bleeding is an important measure to observe.

4.7 Conclusions

In this thesis potential of MWT for detecting intracranial bleedings was tested. Efforts were made to make a realistic phantom of human brain and bleedings, which modeled intracranial bleedings in general and SDH in specific. Initially phantoms were made in plastic buckets followed by making more realistic phantoms in human cranium. The techniques used to make phantoms in this thesis can be used for modeling other types of bleedings. Furthermore, potential interfering factors affecting the performance of the experimental setup were reviewed. Certain trends in raw data have been observed. Moreover, results from the classification algorithm used demonstrates that bleedings can be detected correctly 100% by classifier. Therefore, these results showed that MWT has high potential for detecting intracranial hematomas and may assist other technologies used currently for this purpose.

4.8 Future Outlook

- MWH design and manufacturing process can be improved so MWH assembling process can be done easily.
- Instead of using plastic water bags in MWH a cap which can be filled with water can be designed and manufactured which will serve the same purpose as water bags.
- Efforts should be made to test more interfering factors to experimental setup so that system can be made more stable to achieve goals of portability. Some interesting factors can be testing different length of hair by using wig, temperature effects etc.

- Process of introducing bleeding phantom in human cranium can be improved using other ideas like drilling holes in skull and then putting in bleeding phantom, however, there will be other challenges which need to be fixed.
- Efforts should be made to model other types of bleedings by trying different sizes, shapes and placement of bleedings.

Bibliography

[1] A. D. Gean, N. J. Fischbein, Head trauma (Nov. 2010).
URL http://linkinghub.elsevier.com/retrieve/pii/S1052514910001000?showall=true

[2] J. M. Hardman, A. Manoukian, Pathology of head trauma., Neuroimaging Clin N Am 12 (2) (2002) 175–87, vii.

[3] A. I. R. Maas, N. Stocchetti, R. Bullock, Moderate and severe traumatic brain injury in adults., Lancet Neurol 7 (8) (2008) 728–741.

[4] G. Teasdale, B. Jennett, Assessment of coma and impaired consciousness. a practical scale., Lancet 2 (7872) (1974) 81–84.

[5] M. Bullock, R. Chesnut, J. Ghajar, D. Gordon, R. Hartl, D. Newell, F. Servadei, B. Walters, J. Wilberger, Surgical management of traumatic brain injury, Neurosurgery 58 (2006) S2–1–S2–62.

[6] S. Krishnan, Microwave measurements on brain phantom for brain stroke diagnosis, Master's thesis, Chalmers University of Technology, Gothenburg, Sweden (2011).

[7] M. Khorshidi, T. McKelvey, M. Persson, H. Trefna, Classification of microwave scattering data based on a subspace distance with application to detection of bleeding stroke, in: Computational Advances in Multi-Sensor Adaptive Processing (CAMSAP), 2009 3rd IEEE International Workshop on, 2009, pp. 301 –304.

[8] A. Fhager, X. Zeng, T. Rubaek, H. Dobsicek Trefna, P. Linner, H. Zirath, J. Stake, M. Persson, Progress in clinical diagnostics and treatment with electromagnetic fields, in: Antennas and Propagation (EUCAP), Proceedings of the 5th European Conference on, 2011, pp. 1936 –1937.

[9] P. Rønning, W. Sorteberg, P. Nakstad, D. Russell, E. Helseth, Aspects of intracerebral hematomas–an update., Acta Neurol Scand 118 (6) (2008) 347–361.

[10] J. L. Brisman, J. K. Song, D. W. Newell, Cerebral aneurysms, New England Journal of Medicine 355 (9) (2006) 928–939.
URL `http://www.nejm.org/doi/full/10.1056/NEJMra052760`

[11] C. Badjatia N, Carney N, F. TJ, J. A. ME, Hennes HM, a. L. E. a. M. T. Jernigan S, and Letarte PB, a. S. S. Pons PT, S. T, S. CL, Guidelines for prehospital management of traumatic brain injury, Official journal of the national association 12 Suppl 1 (2008) S1–52.

[12] H. E. Wang, A. B. Peitzman, L. D. Cassidy, P. D. Adelson, D. M. Yealy, Out-of-hospital endotracheal intubation and outcome after traumatic brain injury., Ann Emerg Med 44 (5) (2004) 439–450.

[13] M. J. Rosner, S. D. Rosner, A. H. Johnson, Cerebral perfusion pressure: management protocol and clinical results., J Neurosurg 83 (6) (1995) 949–962.

[14] J. Leon-Carrion, J. M. Dominguez-Roldan, U. Leon-Dominguez, F. Murillo-Cabezas, The infrascanner, a handheld device for screening in situ for the presence of brain haematomas., Brain Inj 24 (10) (2010) 1193–1201.

[15] C. S. Robertson, E. L. Zager, R. K. Narayan, N. Handly, A. Sharma, D. F. Hanley, H. Garza, E. Maloney-Wilensky, J. M. Plaum, C. H. Koenig, A. Johnson, T. Morgan, Clinical evaluation of a portable near-infrared device for detection of traumatic intracranial hematomas., J Neurotrauma 27 (9) (2010) 1597–1604.

[16] A. Fhager, M. Persson, A microwave measurement system for stroke detection, in: Antennas and Propagation Conference (LAPC), 2011 Loughborough, 2011, pp. 1 –2.

[17] S. Gabriel, R. W. Lau, C. Gabriel, The dielectric properties of biological tissues: Ii. measurements in the frequency range 10 hz to 20 ghz., Phys Med Biol 41 (11) (1996) 2251–2269.

[18] S. Semenov, Microwave tomography: review of the progress towards clinical applications., Philos Transact A Math Phys Eng Sci 367 (1900) (2009) 3021–3042.

[19] S. Y. Semenov, D. R. Corfield, Microwave tomography for brain imaging: Feasibility assessment for stroke detection, International Journal of Antennas and Propagation 2008 (2008) 8.

[20] Y. S. Ro, S. D. Shin, J. F. Holmes, K. J. Song, J. O. Park, J. S. Cho, S. C. Lee, S. C. Kim, K. J. Hong, C. B. Park, W. C. Cha, E. J. Lee, Y. J. Kim, K. O. Ahn, M. E. H. Ong, Comparison of clinical performance of cranial computed tomography rules in patients with minor head injury: a multicenter prospective study., Acad Emerg Med 18 (6) (2011) 597–604.

[21] I. G. Stiell, G. A. Wells, K. Vandemheen, C. Clement, H. Lesiuk, A. Laupacis, R. D. McKnight, R. Verbeek, R. Brison, D. Cass, M. E. Eisenhauer, G. Greenberg, J. Worthington, The canadian ct head rule for patients with minor head injury., Lancet 357 (9266) (2001) 1391–1396.

[22] D. Brenner, C. Elliston, E. Hall, W. Berdon, Estimated risks of radiation-induced fatal cancer from pediatric ct., AJR Am J Roentgenol 176 (2) (2001) 289–296.

[23] M. Mazonakis, A. Tzedakis, J. Damilakis, N. Gourtsoyiannis, Thyroid dose from common head and neck ct examinations in children: is there an excess risk for thyroid cancer induction?, Eur Radiol 17 (5) (2007) 1352–1357.

[24] H. Trefna, M. Persson, Antenna array design for brain monitoring, in: Antennas and Propagation Society International Symposium, 2008. AP-S 2008. IEEE, 2008, pp. 1 –4.

[25] A. Gund, S. Lindqvist, Phantom making and modeling of monopole antennas in fd-td for breast cancer studies, Master's thesis, Chalmers University of Technology, Gothenburg, Sweden (2005).

[26] A. F. Ducruet, B. T. Grobelny, B. E. Zacharia, Z. L. Hickman, P. L. DeRosa, K. Anderson, E. Sussman, A. Carpenter, E. S. Connolly, Jr, The surgical management of chronic subdural hematoma., Neurosurg Rev 35 (2) (2012) 155–69; discussion 169.

[27] M. K. N. Seyed Hamed YousefiI Mesri, A multidimensional signal processing approach for classification of microwave measurements with application to stroke type diagnosis, Master's thesis, Chalmers University of Technology, Gothenburg, Sweden (2010).